Nanomedicine And Nanotechnology Journal

SCIENTIFIC LITERATURE

Research Article

Protein Affinity and Effects of Charge-Modified PEGylated Iron-Oxide Nanoparticles on L_β-to-L_α Phase-Transition of DPPC Multilamellar Vesicles: A DSC Study

Goutam Ghosh[1*] and Lata Panicker[2]

[1]UGC-DAE, Consortium for Scientific Research, India

[2]RB & HSD, Bhabha Atomic Research Centre, India

ARTICLE INFO

Received Date: September 08, 2022
Accepted Date: September 27, 2022
Published Date: September 28, 2022

KEYWORDS

PEGylated charged nanoparticles; Counterions; Reverse-charge-parity-counterion interaction; DPPC membrane; Phase transition; DSC

Citation for this article: Goutam Ghosh and Lata Panicker. Protein Affinity and Effects of Charge-Modified PEGylated Iron-Oxide Nanoparticles on L_β-to-L_α Phase-Transition of DPPC Multilamellar Vesicles: A DSC Study. Nanomedicine And Nanotechnology Journal. 2022; 5(1):133

Corresponding author:
Goutam Ghosh,
UGC-DAE Consortium for Scientific Research, Mumbai Centre, India,
Email: ghoshg@csr.res.in; ghoshg@yahoo.com

ABSTRACT

A priori understanding of the interaction of functional nanoparticles with lipid biomembranes can help us to formulate their interaction with human cancer cell membranes. In an earlier report, we proposed a charge-modified PEGylated nanoparticle model for cancer therapy using the "Reverse Charge Parity Counterion Interaction" (RCPC) protocol. The present work is the first step toward developing this model nanoparticle composite. We have examined the protein binding affinity of the unmodified and charge-modified PEGylated Iron-Oxide Nanoparticles (PEG-IONPs) using ζ-potential and the secondary conformations of the interacted proteins using Circular Dichroism (CD). The effects of these without or with protein-bound nanoparticulates on the L_β-to-L_α phase-transition of zwitterionic Dipalmitoyl Phosphatidylcholine (DPPC) Multilaminar Vesicles (MLVs) were studied using Differential Scanning Calorimetry (DSC). Pre-synthesized PEG-IONPs have been modified with counterion-conjugated cationic or anionic molecules such as I^- conjugated Cetylpyridinium Iodide (CPI) or Li^+ conjugated Tri-Lithium Citrate (TLC), respectively. These nanoparticulates become applicable for Reverse-Charge-Parity-Counterion (RCPC) interaction.

INTRODUCTION

Recent reports [1-4] suggest that the research towards applications of functional nanoparticulates in the diagnosis and therapy of cancer still demands exploration of various aspects such as the effect of nanoparticle size, shape, surface chemistry, and protein corona for achieving goals like targeting specific cells and cellular uptake, and understanding the toxicity to normal cells [5,6]. These aspects are the major hurdles toward the development of nanomedicine. Moreover, cancer cell membranes are complex systems, and the complexities vary from one type of cancer cell to the other [7]. Some of these aspects regarding nano-bio interaction are easier to address with model phospholipid membranes that mimic the cell membranes of normal cells and the functional nanoparticles with desired goals [7-9].

The phospholipid-based model membranes, such as zwitterionic Dipalmitoyl Phosphatidylcholine (DPPC), are self-assembled bilayer structures of amphiphilic lipid molecules, each has an ionic head group (hydrophilic) and two acyl chains (hydrophobic). Acyl chains in the layered assemblies face each other, and the head groups on both sides are in contact with the aqueous solvent. At room temperature, the acyl chains remain in an extended trans conformation forming a tilted 2D ordered

lattice in the lamellae, called the gel phase (L_β). Above the chain melting temperature (T_m), the acyl chains start losing their cooperativity (ordering) and finally transform into a completely disordered 2D fluid or liquid phase (L_α), which allows diffusion of foreign elements through it. This transition is called L_β-to-L_α phase-transition, which passes through an intermediate ripple phase ($P_{\beta'}$) – gel and fluid phases coexist, and tilting of acyl chains vanishes – at a pretransition temperature (T_{PT}) [10]. Cartoons in Figure 1 depict different conformations of a bilayer membrane upon heating. Vesicles could be either spherical cages of a single lipid bilayer encapsulating the aqueous solvent, called Unilamellar Vesicles (ULVs), or concentric spheres of multiple lipid bilayers separated by the aqueous solvent, called Multilamellar Vesicles (MLVs) [11].

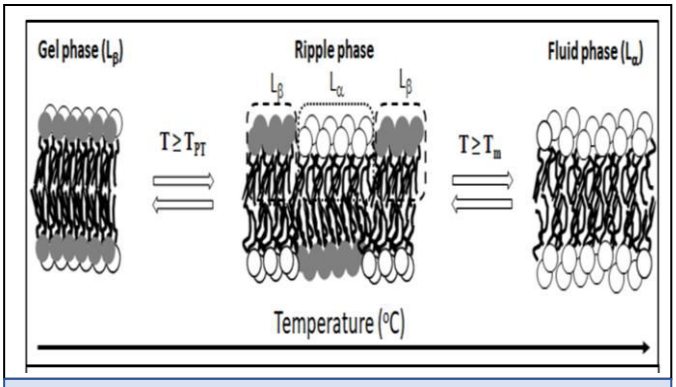

Figure 1: Pictorial depiction of the phases of DPPC membrane with increasing temperature.

Many groups have reported their research on nanoparticle-lipid membrane interaction; for example, Torrano et al. [7] have reported the interaction of oppositely charged gold nanoparticles with DPPG and DPPC Langmuir Monolayers (LMs), which was dominantly electrostatic, resulting in the changes of elasticity of both LMs. Several studies have reported on the effects of inorganic NPs on fluidity, i.e., softening or stiffening of lipid bilayers, which depends on factors like chemical identity, size, and shape of nanoparticles [12,13]. Pattani et al. [10] have reported that the interaction of chitosan nanoparticles with the polar head groups of DPPC MLVs has inhibited the formation of the intermediate ripple phase ($P_{\beta'}$), and the intercalation of nanoparticles into the acyl chain region has reduced the cooperativity and broadened the DSC endotherms of their melting transitions.

Pfeiffer et al. [14] used Laser Scanning Confocal Microscopy (LSCM), FCS, and X-Ray Reflectivity (XRR) and the Molecular Dynamics (MD) simulation to understand the effect of absorption of cationic gold nanoparticles (AuNPs) on the structure and dynamics of a mixed (1:1) anionic (POPG)/zwitterionic (POPC) lipid membranes. They reported a strong electrostatic attraction between cationic AuNPs and anionic membranes, together with an entropic contribution due to counterion effects, drove strong adhesion of AuNPs on the biomimetic membrane, and from MD simulation, the nanophase separation when NPs adhered to the membrane lipids. This lateral phase separation has caused the formation of negatively charged patches within the membrane, as per the report.

For the interaction of anionic nanoparticles with model zwitterionic lipid membranes, surface charges contribute to the electrostatic repulsion, while hydrophobicity drives the possible embedding of nanoparticles inside the membrane [15-17]. Piosik et al. [18] reported the influence of native and aminated starch-coated magnetite (Fe_3O_4) nanoparticles on the thermodynamics, morphology, and dilatational elasticity of DPPC LMs and showed that the presence of the amine group on nanoparticles has reduced the disruptive effect of the magnetite nanoparticles on the model membranes and improved their adsorption. Using an atomistic Molecular Dynamics (MD) simulation, Allen et al. [19] have inferred that the permeation of monovalent ions through lipid membranes can occur due to the formation of ion-induced defects in the membrane; defects form through membrane perturbations due to movements of ions.

Among several techniques used for the characterization of lipid morphology, Differential Scanning Calorimetry (DSC) [20,21] is the one that provides a sensitive means of detecting phase transition temperatures (T_m), such as the gel-to-liquid (L_β-to-L_α) transition of lipid vesicles, and their associated enthalpies, which reflect their packing properties and alkyl chain conformations. Earlier, we reported the irreversible denaturation of the secondary conformations of proteins due to "Reverse Charge Parity Counterions" (RCPC) interaction with counterion-conjugated charged iron-oxide nanoparticles (ccc-IONPs) [22-24]; in one of those studies [22], we used DSC technique to confirm the unfolding of proteins after interaction

Protein Affinity and Effects of Charge-Modified PEGylated Iron-Oxide Nanoparticles on Lβ-to-Lα Phase-Transition of DPPC Multilamellar Vesicles: A DSC Study. Nanomedicine And Nanotechnology Journal. 2022; 5(1):133.

with nanoparticles. In the RCPC interaction, the charged nanoparticles electrostatically bind with the oppositely charged substrates like proteins or biomembranes and subsequently release counterions which intercalate into the substrates and rupture them. The RCPC interaction and the necrotic death of lymphoblastoid Raji cells through lysis of the cell membrane after interaction with ccc-IONPs has been reported earlier, where the membrane lysis explained in terms of the entropy-driven hole formation upon intercalation of counterions [6].

In a recent paper [25], we proposed a model functional nanoparticle composite for the core (e.g., Fe_3O_4) surface-coated with: (1) Polyethylene Glycol (PEG) to protect the nanoparticulates from "protein corona" formation, (2) counterion-conjugated charged molecules to execute RCPC interaction with the cell membranes, (3) appropriate antibody for specific binding to cancer cells, and (4) fluorescence dye to locate nanoparticulates at the targeted organs in the body. The proposed nanoparticle composite can be developed through a step-by-step strategy; the present study marks the first step.

Therefore, in the present study, we aimed to study the RCPC interaction of PEG-coated ccc-IONPs with a model lipoprotein vesicle such as Multilamellar Vesicle (MLV) of zwitterionic dipalmitoyl phosphatidylcholine (DPPC) which mimics a cell membrane using the Differential Scanning Calorimetry (DSC) technique. We modified the pre-synthesized PEGylated IONPs (PEG-IONPs) with (i) counterion-conjugated anionic Tri-lithium citrate (TLC) and (ii) counterion-conjugated cationic Cetylpyridinium iodide (CPI), and examined the RCPC interaction, first, with standard proteins, e.g., hen egg white lysozyme (Lys) and pepsin A (PSA), respectively, which express net positive or negative surface charge. After confirming RCPC interaction between ccc-PEG-IONPs and proteins and examining the protein binding affinity to these PEGylated IONPs, we planned to study RCPC interaction between ccc-PEG-IONPs and DPPC MLVs in terms of the changes in their DSC endotherm profile during gel-to-fluid phase (L_β-to-L_α) transition. We have also used protein-bound ccc-PEG-IONPs to study the RCPC interaction with DPPC MLVs.

MATERIALS AND METHODS

We used pre-synthesized polyethylene glycol (PEG, M.W. ~6000) coated iron oxide nanoparticles (PEG-IONPs) [22] for surface modification with anionic Tri-Lithium Citrate (TLC) and cationic Cetylpyridinium Iodide (CPI), respectively. TLC ($Li_3C_6H_5O_7$, 98.5%) was purchased from S. D. Fine Chem. Ltd., Mumbai, India, and CPI ($C_{21}H_{38}IN$, 98%) were purchased from Sigma-Aldrich, India. Hen egg white lysozyme (Lys, $<M_W>$ =14,300 $g.mol^{-1}$; L-6876, Grade-1) and Pepsin A (PSA, $<M_W>$ = 345,000 $g.mol^{-1}$; P6887) were purchased from Sigma, USA. Sodium phosphate, pH 7.4, the buffer was made using analytical grade dibasic sodium phosphate (Na_2HPO_4, $2H_20$) and monobasic sodium phosphate (NaH_2PO_4, H_20). Dipalmitoyl Phosphatidylcholine (DPPC) was purchased from Avanti polar Lipids, Birmingham, Alabama, USA. All chemicals were used without any further purification. The Milli-Q water, obtained from a three-stage purification system (Millipore, USA), was further filtered through a 0.22-micron filter and then autoclaved, which showed pH and the electrical resistivity 6.5 and 18.2 $M\Omega.cm^{-1}$, respectively. This water was used for sample preparations.

Charge modification of PEG-IONPs

Pre-synthesized PEG-IONPs were charge-modified with TLC and CPI. For this, powders of TLC or CPI and dried PEG-IONPs were taken at a 1:1 weight ratio and dispersed in Milli-Q water under continuous sonication for 3-4 hours. The sonicated black precipitates were washed 4-5 times to remove free ionic molecules from the dispersion. These charge-modified PEG-IONPs were then dried at room temperature and then dispersed in Milli-Q water to make 1% (w/v) dispersions of TLC-modified anionic PEG-IONPs (TLC-PEG-IONPs) and CPI-modified cationic PEG-IONPs (CPI-PEG-IONPs) for further experiments.

Preparation of protein solutions and incubation with nanoparticles

The stock solutions of lysozyme and pepsin A were prepared in 0.1% w/v concentration in water by dissolving 1 mg protein in 1 ml of Milli-Q water. The stock solutions of nanoparticles in water were diluted to 0.1% w/v for incubation with proteins. The nanoparticles and proteins were mixed in the 1:1 v/v ratio and left for 48 hours of incubation to ensure the equilibrium state of protein adsorption/desorption on nanoparticles [22,23]. Afterward, the dispersion was diluted to make the final concentration of proteins and nanoparticles 0.033% (w/v) in the reaction mixture.

Protein Affinity and Effects of Charge-Modified PEGylated Iron-Oxide Nanoparticles on Lβ-to-Lα Phase-Transition of DPPC Multilamellar Vesicles: A DSC Study. Nanomedicine And Nanotechnology Journal. 2022; 5(1):133.

Preparation DPPC MLVs in phosphate buffer

Dipalmitoyl Phosphatidylcholine (DPPC) vesicles were used as artificial membranes because of their biomimetic properties. Multilamellar Vesicles (MLVs) of DPPC (13.6 mM or 10 mg/ml) were formed using the lipid film hydration method. The lipid film was hydrated with pH 7.4 sodium phosphate buffer. A thorough dispersion of DPPC in the buffer was achieved by 10 times repeating the heating in a water bath maintained at 10°C above the chain-melting temperature and vortexing at room temperature. These steps were repeated at least 10 times. To this DPPC dispersion, we added (a) unmodified or charge-modified PEG-IONPs dispersions and (b) protein-coated unmodified or charge-modified PEG-IONPs dispersions in a 10:1 weight ratio and studied their effects on the L_β-to-L_α phase-transition of the zwitterionic DPPC MLVs using the differential scanning calorimetry.

X-Ray diffraction (XRD)

X-Ray Diffraction (XRD) scan of the powder PEG-IONPs was collected at 25 °C using a Bruker D2 Phaser (USA) desktop diffractometer. The sample was loaded in a grooved glass substrate.

Dynamic light scattering (DLS) and zeta-potential

The size and size distribution of PEG-IONPs, TLC-PEG-IONPs, and CPI-PEG-IONPs were measured at 25°C, and the zeta-potential (ζ-potential) of unmodified, TLC- and CPI-modified PEG-IONPs before and after incubation with Lys and PSA was measured at 25 and 45 °C using a DLS Zetasizer nano Z (Malvern, UK) instrument. Each sample was diluted to avoid the multi-scattering effect and loaded in a dip-cell with copper electrodes and at least 3 runs were taken for statistical data. In the Table, we presented average data with error bars.

Circular dichroism (CD)

The secondary conformation of Lys and PSA before and after interaction with unmodified and charge-modified PEG-IONPs was measured at 25°C using a JASCO, J-815 (Japan) Circular Dichroism (CD) instrument in the wavelength range of 195–260 nm. At least 3 runs were taken for each sample; the average of three has been presented in the Table with error bars. CDNN®2.1 software, provided by the company, was used to analyze the secondary folding of proteins.

Differential scanning calorimeter (DSC)

The Mettler Toledo DSC 822e differential scanning calorimeter was used for thermal measurements of the membrane samples, with an empty aluminum pan as a reference; temperature and enthalpy calibration of the instrument was performed using cyclohexane and indium at a heating rate of 10°C/min. For DSC measurements, 25 to 30 mg of MLVs without or with nanoparticles were hermetically sealed in aluminum pans, and measurements were carried out with a heating rate of 5 °C/min. The Chain-Melting (CM), Transition Temperature (T_m), and transition enthalpy (ΔH_m) of the DPPC membrane were obtained using the heating endothermic curve; the full width at half-maximum to compare the cooperativity of the CM transitions was obtained from the heat flow versus temperature scans; experiments conducted immediately following the preparation of MLVs. The measurement for each sample was repeated at least 3 times, and the results reported here indicate the average of three with error bars indicating the average variance among the three measurements.

RESULTS AND DISCUSSION

X-Ray diffraction (XRD)

To verify the stability of the Fe_3O_4 phase, we collected the XRD pattern of the dried powder of the old PEG-IONPs (prepared in 2013, [22]) and compared this pattern with the XRD pattern of uncoated IONPs reported earlier [22] as shown in Figure S1 in the Supplementary Information (SI). Excellent matching of the XRD peaks confirms the stability of the Fe_3O_4 phase of nanoparticles after aging of 10 years in an aqueous medium. However, the PEG-IONPs XRD pattern has a broad polymer background and reduced peak intensities compared to the uncoated IONPs pattern, which is expected. Using the measured widths of low and high 2θ peaks and the Scherrer formula, we estimated the average grain size of PEG-IONPs around 30 ± 1 nm. The particle sizes of PEG-IONPs, TLC-PEG-IONPs, and CPI-PEG-IONPs in aqueous dispersions were measured using DLS, which are comparable with the grain size obtained from the XRD pattern of PEG-IONPs.

Size of unmodified and charge-modified PEG-IONPs

Using the dynamic light scattering technique, we have measured the size of unmodified and charge-modified PEG-IONPs. The representative figures of size and size distributions of PEG-IONPs, TLC-PEG-IONPs, and CPI-PEG-IONPs are given

Protein Affinity and Effects of Charge-Modified PEGylated Iron-Oxide Nanoparticles on Lβ-to-Lα Phase-Transition of DPPC Multilamellar Vesicles: A DSC Study. Nanomedicine And Nanotechnology Journal. 2022; 5(1):133.

in the SI. The hydrodynamic diameters of PEG-IONPs and TLC-PEG-IONPs, measured using DLS, were in the range of 30–40 nm, which closely matches the grain size of PEG-IONPs and is in good agreement with our earlier report on PEG-IONPs [22]. It indicates the stability of PEG-IONPs after a decade of aging and the goodness of TLC coating on PEG-IONPs. The hydrodynamic diameter of CPI-PEG-IONPs has been measured to be approximately 65 nm, which indicates an agglomeration of nanoparticulates because it is double in diameter compared to the grain size measured using XRD.

Zeta-potential

The Zeta-potential (ζ-potential at 25 and 45°C) of unmodified, TLC, and CPI-modified PEG-IONPs before and after incubation with Lys and PSA are shown in Table 1. The unmodified PEG-IONPs showed negative values at both temperatures because of the dangling OH^- functional groups of PEG molecules on IONPs. Citrates are anions, thus resulting in a negative ζ-potential at both temperatures to the TLC-modified PEG-IONPs (TLC-PEG-IONPs); on the other hand, Cetylpyridinium is a cationic surfactant, therefore contributed to a positive ζ-potential of the CPI-modified PEG-IONPs (CPI-PEG-IONPs) at the two temperatures.

Table 1: ζ-potential data of unmodified, and TLC and CPI-modified PEG-IONPs.

Dispersions	Temperature (°C)	ζ-potential (mV)	Δζ (mV) after protein binding	Approx. no. of bound proteins
PEG-IONPs	25	–6.5 ± 0.5	--	N.A.
	45	–31.3 ± 1.2	--	N.A.
TLC-PEG-IONPs	25	–26.4 ± 0.8	--	N.A.
	45	–26.3 ± 0.5	--	N.A.
CPI-PEG-IONPs	25	+10.0 ± 1.1	--	N.A.
	45	+6.0 ± 0.6	--	N.A.
Lys/PEG-IONPs	25	+3.5 ± 0.3	+10.0	2
	45	+0.7 ± 0.1	+32.0	6
PSA/PEG-IONPs	25	–7.2 ± 0.3	–0.7	Nil
	45	–33.3 ± 2.1	–2.0	Nil
Lys/TLC-PEG-IONPs	25	–6.1 ± 0.3	+20.3	4
	45	–9.9 ± 0.9	+16.4	3
PSA/TLC-PEG-IONPs	25	–11.9 ± 1.3	+14.5	?
	45	–11.7 ± 0.7	+14.6	?
Lys/CPI-PEG-IONPs	25	+11.6 ± 0.8	+1.6	Nil
	45	+11.0 ± 0.1	+5.0	1
PSA/CPI-PEG-IONPs	25	–2.4 ± 0.3	–12.4	0.5
	45	–6.5 ± 0.2	–12.5	0.5
DPPC MLVs	25	–1.2 ± 0.1	--	N.A.
	45	–2.5 ± 0.1	--	N.A.

Isoelectric Points (IEPs) of Lys and PSA are around 10.7 and 3.2. Therefore, in water dispersions (pH 6.5), they show positive (+4.8) and negative (–23.7) ζ-potentials, respectively, at 25 °C [26]. According to earlier reports [27-30], PEG coating prevents the formation of "protein corona" and preserves the targetability of functional nanoparticles for *in vivo* applications. However, the reverse charge parity interaction [22] suggests the binding of Lys on PEG-IONPs and TLC-PEG-IONPs as both show negative ζ-potentials and PSA on CPI-PEG-IONPs as it shows positive ζ-potential, and accordingly, either reducing the value or changing the sign of the ζ-potential of nanoparticles as shown in Table 1. The ζ-potential of DPPC MLVs at both temperatures was negative, as given in Table 1.

The differences in ζ-potentials (Δζ) of nanoparticles before and after protein binding have been listed in Table 1, which gives a rough estimation of the number of bound proteins on nanoparticles. These numbers appear substantially low as compared to the numbers of proteins in the close-packed binding (i.e., CPB = Surface area of a coated nanoparticle / Cross-section of a protein) calculations; for example, CPB of Lys (diameter ~1.8 nm [26]) on a TLC-PEG-IONP (considering diameter ~32 nm) could be as high as ~1000 and PSA (diameter ~3.2 nm [26]) ~400. Therefore, binding a few proteins even on PEGylated nanoparticles cannot be prevented, though this may not affect the functionality of nanoparticles. Moreover, a heftier protein like PSA did not show noticeable binding on either unmodified or charge-modified PEG-IONPs, at all temperatures supporting the benefit of PEGylation. In the case of PSA/TLC-PEG-IONPs (Table 1), the reason for protein binding is unclear because PSA binding cannot cause a positive Δζ; moreover, reverse charge parity interaction does not allow PSA binding on TLC-PEG-IONPs. So, these values of Δζ may indicate the detachment of a few TLC molecules from the surface of TLC-PEG-IONPs.

Circular dichroism (CD)

The Circular Dichroism (CD) plots are shown in Figure S2 in SI. These measurements showed changes in the secondary conformations of proteins after interaction with unmodified and charge-modified PEG-IONPs; the significant unfolding was

explained using the RCPC interaction model [22-24]. Table 2 shows the data of the secondary conformations of Lys and PSA before and after interaction with nanoparticulates as analyzed from CD plots.

Table 2: Secondary conformations (%) of proteins before and after interaction with nanoparticles.

Proteins before and after interaction with nanoparticles	% α-helix	% β-sheet (antiparallel)	% Random coil
Lys	12.6 ± 1.2	29.7 ± 0.8	33.2 ± 0.6
Lys / PEG-IONPs	12.7 ± 1.3	28.8 ± 0.7	33.4 ± 0.4
Lys / TLC-PEG-IONPs	11.2 (*) ± 0.3	32.3 ± 0.3	33.1 ± 0.8
Lys / CPI-PEG-IONPs	12.7 ± 0.6	29.1 ± 0.2	33.2 ± 0.6
PSA	11.2 ± 0.4	29.7 ± 0.5	34.6 ± 0.2
PSA / PEG-IONPs	11.2 ± 0.4	29.8 ± 0.5	34.3 ± 0.6
PSA / TLC-PEG-IONPs	11.0 ± 0.6	27.1 ± 0.2	35.7 ± 0.1
PSA / CPI-PEG-IONPs	10.2 (*) ± 0.1	34.0 ± 0.1	33.1 ± 0.3

Table 2 confirms the RCPC interaction and unfolding of the α-helix conformation of Lys and PSA, shown by the asterisk marks (*), even with their low binding affinity to the charge-modified PEG-IONPs. Therefore, we can infer that the PEG coating on charged nanoparticles did not hinder the RCPC interaction. Using DSC, we examined the RCPC interaction of these PEG-IONPs without or with protein conjugation with the zwitterionic DPPC MLVs and the corresponding effect on the L_β-to-L_α phase-transition of lipid membranes.

Differential scanning calorimetry (DSC)

The chain melting temperature (T_m) of pure DPPC MLVs was around 40.76 °C, which is in close agreement with an earlier report [10]. We have investigated the effect of proteins (native) on the L_β-to-L_α phase transition of DPPC MLVs (Figure S3 in SI) and observed that the interaction with Lys slightly reduced (~40.66 °C) the chain melting temperature (T_m), whereas PSA did not cause recognizable effect. We conjecture that Lys, being positively charged molecules (positive ζ-potential), accumulated around the negative head group sites, neutralized the surface charge of DPPC, and allowed hydration at the chain region, reducing the cooperativity that lowered the T_m.

Figure 2 shows the DSC endotherms of DPPC MLVs between 38 and 44° C, representing the gel-to-liquid (L_β-to-L_α) phase transition before and after interaction with (a) unmodified and (b, c) charge-modified PEG-IONPs without or with protein conjugation. At a glance, each figure appears different from the others, as explained below.

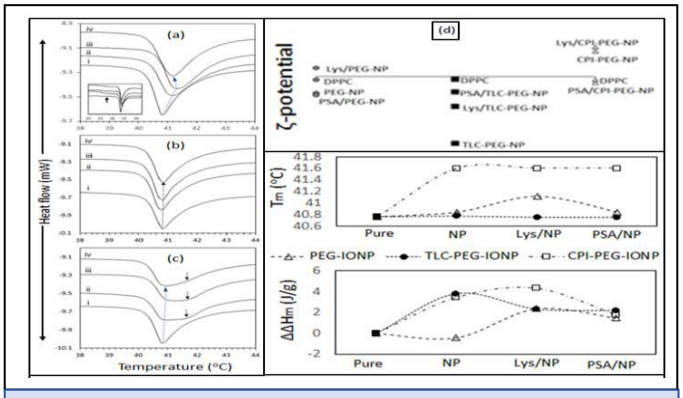

Figure 2: DSC endotherms of $L_\beta \rightarrow L_\alpha$ transition of DPPC MLVs as (i) pure and after interaction with (ii) bare, and (iii) Lys and (iv) PSA conjugated nanoparticulates: (a) PEG-IONPs, (b) TLC-PEG-IONPs, and (c) CPI-PEG-IONPs; (d) top plate: ζ-potential of pure DPPC MLVs and NPs without and with protein conjugations; middle plate: T_m, and bottom plate: $\Delta\Delta H_m$ of the transition before and after interaction with bare (NP) and protein conjugated NPs (protein/NP). Identities of differently coated IONPs have been represented by different symbols as given in the legends.

Table 3 gives thermal parameters of the L_β-to-L_α phase transitions in DPPC MLVs (without and with additives): chain-melting temperature T_m, change in T_m (ΔT_m), and transition enthalpy ΔH_m and change in ΔH_m ($\Delta\Delta H_m$) compared to pure DPPC before and after interaction with unmodified or charge-modified PEG-IONPs and those with protein conjugation. ΔT_m and $\Delta\Delta H_m$ values represent the change in the membrane organization compared to that of the native state. Note that a positive ΔT_m suggests an increase in the melting temperature of the L_β-to-L_α transition of the DPPC membrane. The change in enthalpy (ΔH_m) is proportional to the heat absorbed during the transition, and a positive $\Delta\Delta H_m$ suggests the absorption of more heat; in other words, the gel phase of the DPPC membrane became more stable. Keeping these in mind, DSC data have been analyzed.

Table 3: DSC data of DPPC without or with unmodified and charge-modified PEG IONPs without or with protein conjugation.

Sample	T_m (°C)	ΔT_m (°C)	ΔH_m (J/g)	$\Delta\Delta H_m$ (J/g)
DPPC pure	40.76 ± 0.3	---	38.61 ± 0.5	0
DPPC + PEG-IONPs	40.84 ± 0.2	0.08	38.19 ± 0.8	– 0.42
DPPC + Lys/PEG-IONPs	41.11 ± 0.5	0.35	40.97 ± 1.0	+ 2.36
DPPC + PSA/PEG-IONPs	40.84 ± 0.1	0.08	40.06 ± 0.4	+ 1.45
DPPC + TLC-PEG-IONPs (Li^+)	40.77 ± 0.5	0	42.41 ± 0.2	+ 3.80
DPPC + Lys/TLC-PEG-IONPs (Li^+)	40.75 ± 0.6	0	40.93 ± 0.5	+ 2.32
DPPC + PSA/TLC-PEG-IONPs (Li^+)	40.75 ± 0.1	0	40.80 ± 0.8	+ 2.19
DPPC + CPI-PEG-IONPs (I^-)	40.75 ± 0.5 41.6 ± 0.2	0, 0.84	42.03 ± 0.6	+ 3.42
DPPC + Lys/CPI-PEG-IONPs (I^-)	40.75 ± 0.1 41.6 ± 0.1	0, 0.84	42.91 ± 0.8	+ 4.30
DPPC + PSA/CPI-PEG-IONPs (I^-)	40.75 ± 0.3 41.6 ± 0.2	0, 0.84	40.35 ± 1.0	+ 1.74

(Li^+) and (I^-) represent lithium and iodine counterions in the respective dispersions.

Figure 2(a) shows the chain melting endotherms of DPPC MLVs upon interaction with bare or protein-conjugated unmodified PEG-IONPs. Two distinct features are evident in these endotherms: (i) noticeable shifts of T_m toward higher temperatures after interaction with nanoparticles, which suggests, in general, an increase in the head group rigidity of the DPPC membranes [7,10], and (ii) broadening of the transition endotherms, implying a reduction in the cooperativity among the lipid acyl chains [10]. The inset shows the same DPPC endotherms in the temperature range of 30 and 48 °C, where each endotherm shows both the gel-to-ripple phase transition at T_{PT} (~36 °C) and the chain melting transition at T_m (~41 °C) before and after interaction with nanoparticles. It indicates that nanoparticles did not affect the intermediate phase of DPPC, which contradicts an earlier report [10].

According to Pattani et al. [10], the above two distinct features of the chain melting transition of DPPC could be associated with the intercalation of nanoparticles between the lipid polar head groups by forming hydrogen bonds and/or by electrostatic interaction and also penetration into the cooperative region. Table 1 shows that the ζ-potential of both DPPC MLVs and PEG-IONPs were negative (–2.5 mV and –31.3 mV, respectively, at 45 °C). So, they could only electrostatically repel each other and restrict the movement of head groups creating a membrane ordering compared to the native DPPC MLVs. Because of this electrostatic repulsion, PEG-IONPs were not expected to intercalate into the membrane, and, therefore, the broadening of the chain melting transition cannot be explained in terms of nanoparticle penetration into the cooperative region. Based on an earlier report [31], we conjecture that the transition at T_m was a "non-two-state" gel-to-liquid transition where the intermediate "ripple phase" (Figure 1) formed non-uniform clusters of lipid molecules in the bilayer with a few regions more ordered and denser due to excessive dehydration. Thus, the transition to the liquid phase got shifted to a higher temperature compared to pure DPPC. This "non-two-state" model can nicely explain the asymmetry of the chain melting endotherm. The shift of T_m was maximum for Lys/PEG-IONPs + DPPC MLVs system. From Table 1, we can see that the ζ-potential of Lys/PEG-IONPs was positive, which matches the scenario of the chitosan and DPPC MLVs interaction reported by Pattani et al. [10] for positive ζ-potential [32,33] of chitosan NPs, and so, their explanation also may apply in this specific case.

Since PSA did not bind on PEG-IONPs, the DPPC + PSA/PEG-IONPs and the DPPC + PEG-IONPs scenarios were nearly identical, and thus both samples did produce identical DSC endotherms.

Figure 2(b) shows the chain melting (L_β-to-L_α) endotherms of DPPC MLVs before and after interaction with bare or protein-conjugated TLC-PEG-IONPs; all appear similar, suggesting no interaction between vesicles and nanoparticulates. This result contradicts the scenario of DPPC + unmodified or protein conjugated PEG-IONPs system. Although in both cases, nanoparticulates had negatively charged surfaces, the difference may occur due to counterion (Li^+) condensation, similar to a micellar system reported earlier [34], around the TLC-PEG-IONPs composites in the repulsive force field with DPPC MLVs, which effectively screened the surface charge of nanoparticulates and turned them inactive for electrostatic interaction with the DPPC head groups.

Figure 2(c) shows the chain melting endotherms of DPPC MLVs before and after interaction with bare or protein-conjugated CPI-PEG-IONPs. These endotherms are different from the

previous two scenarios. In these endotherms, we can notice two distinct chain melting temperatures, e.g., at around 40.75 °C and 41.6 °C, the second melting transition is prominent in the endotherms (ii) and (iii) for DPPC + CPI-PEG-IONPs and DPPC + Lys/CPI-PEG-IONPs samples, respectively, while it is less in the endotherm (iv) for DPPC + PSA/CPI-PEG-IONPs sample. In Figure 2(a), for PEG-IONPs without counterions, the L_β-to-L_α transition profile has broadened due to reduced cooperativity between the acyl chains of the intermediate ripple state [10], but it was progressively transforming. In Figure 2(c), in the presence of I^- counterions, the two clear minima suggesting domain formation [35] in the membrane, one melted at normal T_m of pure DPPC (~40.75 °C) while the other melted at a higher temperature (~41.6 °C), the two are separated by 0.85 °C. We have denoted the lower T_m gel domain as "soft gel" and the higher T_m domain as "hard gel", separated by the fluid region of the membrane. Electrostatic binding of cationic NPs at the zwitterionic DPPC surface and the subsequent counterion effect was also reported by Pfeiffer et al. [14]. The different domain formation during the phase transition has been shown in Figure 3.

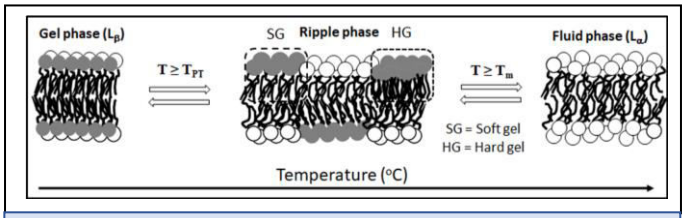

Figure 3: Modified picture of the membrane phase transformation.

In Figure 2(d), the top plate shows the ζ-potentials of pure DPPC MLVs and NPs without and with protein conjugations, the middle plate shows the chain melting temperature (T_m) of DPPC MLVs before and after interaction with bare (NP) and protein conjugated NPs (protein/NP), and the bottom plate shows the change in the transition enthalpy ($\Delta\Delta H_m$) relative to that of the pure DPPC MLVs before and after interaction with NP and protein/NP. ζ-potential (top plate) of DPPC MLVs in sodium phosphate buffer (pH 7.4) was found negative, which is in agreement with an earlier report [36]. The ζ-potentials of Lys/PEG-NP, CPI-PEG-NP, and Lys/CPI-PEG-NP were positive. Therefore, these nanoparticle composites were expected to undergo RCPC interaction with DPPC MLVs, which was confirmed by the DSC results. Two transition temperatures have been observed in DSC endotherms when DPPC interacted without and with Lys conjugated CPI-PEG-IONPs; this has been explained above due to the formation of two different gel phases. The chain melting temperature (T_m) of DPPC MLVs (middle plate) has also been seen to increase after interaction with Lys/PEG-NP, CPI-PEG-NP, Lys/CPI-PEG-NP, and PSA/CPI-PEG-NP, which supports the existence of an intermediate "hard gel" phase as explained above. The change in the transition enthalpy ($\Delta\Delta H_m$) compared to that of the pure DPPC MLVs before and after interaction with NP and protein/NP (bottom plate) also agrees with above results.

The formation of two different gel domains was probably the consequence of the intercalation and non-uniform distribution of counterions (I^-) in the acyl chain regions once CPI-PEG-IONPs were bound electrostatically [14,37] and neutralized the surface charge of the DPPC membrane, according to the RCPC interaction model [24]. Usually, the charge transport across lipid membranes is regulated by specific channels and transporters; however, the uncatalyzed ions', such as alkaline metal and halides, permeation through lipid membranes has also been reported through deformation in the lipid membrane due to the movement of charges [19,38-40]. Chakraborty et al. [41] reported that the lipid membrane with an unsaturated chain exhibits a very small affinity toward metal ions. Since DPPC has no unsaturated chain [42], we expected the interaction of Li^+ ions with membranes in the DPPC + TLC-PEG-IONPs without or with protein conjugation samples. However, from Figure 2(b) of DSC endotherms, we could not notice any effect of Li^+ in the DPPC membrane, which can be justified only using the RCPC interaction model, which requires oppositely charged bodies to bind electrostatically to release conjugated counterions. Thus, without and with protein-conjugated anionic TLC-PEG-IONPs did not bind with the anionic DPPC surface, and therefore, there were no free counterions to intercalate into the membrane for the implementation of the RCPC interaction.

CPI-PEG-IONPs and Lys/CPI-PEG-IONPs with positive surface charges can electrostatically bind with the negative headgroups at the surfaces of DPPC MLVs and release anionic (I^-) counterions. The released counterions can cause two effects: (1) intercalate into the hydrophobic chain region of the lipid

bilayer, with an attached hydration layer [41], due to surface charge neutralization and reduction of the permeation energy barrier for ions, or (2) bind with the nearby positive headgroups where cationic nanoparticulates bound in the surface region.

Bangham et al. [43], in an investigation of the diffusion of univalent ions across the lamellae of swollen phospholipids, reported that the diffusion rate of anions (e.g., I^-) through biomembrane was many orders of magnitude more than that of cations (e.g., Li^+). They also reported that the diffusion rate of cations is largely controlled by the sign and magnitude of the surface charge at the water/lipid interface, and it decreases as the negative charge on the lipid structure decreases. However, the diffusion rate of anions remained very high, which may explain why we did observe so much difference between the endotherms during the L_β-to-L_α transition of DPPC MLVs after interaction with TLC-PEG-IONPs (Figure 2a) and CPI-PEG-IONPs (Figure 2c).

The intercalated hydrated counterions (I^-) probably accumulated nonuniformly in a few regions and created local static electric fields. This electric field can distort the bond angles of the pulled water molecules and create a local anisotropy in the electric field. The local anisotropic electric field can polarize the hydrocarbon chain molecules of lipids defferently depending on the field direction and orientations of the hydrocarbon bonds in the molecules, similar to those of the hydrophobic nanopores or cavities reported earlier using the MD simulations [44,45]. Consequently, the chains in some regions stiffen more than those in areas where there was no or fewer counterions accumulation; this may explain why there were HG and SG regions surrounded by the liquid phase in the core of the DPPC membranes, as shown in Figure 3.

Another possibility is that anionic counterions can bind with a few positive headgroups to neutralize their charge and reduce the surface area. The reduced headgroup area results in a significantly lower area per lipid, as reported for the DPPE membrane [46], at a few random regions making the membrane structure HG with highly ordered hydrocarbon lipid chains compared to the other SG regions shown in Figure 3. Consequently, there are two distinct melting temperatures in the DSC endotherms in Figure 2(c).

Thus, while Figure 1 can explain the phase transition endotherms of DPPC MLVs in Figures 2(a) and 2(b), it needs to modify, as shown in Figure 3, to explain the transition endotherms in Figure 2(c). At higher temperatures, when the counterions were thermally dispersed or moved out of the membrane, the local electric fields decayed, and the conformation of the gel phases transformed into the liquid phase. Based on the above heuristic arguments, we can claim that the RCPC interaction has worked with the charge-modified PEG-IONPs and the model phospholipid membrane system of DPPC MLVs. It approves the success in the initial step toward developing the model nanoparticulates for cancer therapy proposed by us recently [25].

CONCLUSIONS

In this work, we PEGylated charged Iron Oxide Nanoparticles (IONPs) as the first step in developing our proposed model nanoparticle system for cancer therapy as propsed in our earlier publication. We chose the zwitterionic DPPC phospholipid-based MLVs as simple biomimetic model membranes representing the cancer cell membranes. We examined the affinity of protein binding on these PEGylated charged IONPs and their RCPC interaction with the DPPC MLVs in terms of the gel-to-liquid phase transition of the lipid membranes using several experimental techniques, as mentioned in earlier sections. The DSC results obtained indeed indicate the reverse charge binding of charge-modified PEG-IONPs with the head region of the DPPC MLVs and intercalation of the released anionic counterions into the hydrophobic core of the membrane that created the “Hard Gel” (HG) phase in coexistence with the “Soft Gel” (SG) phase in the DPPC membrane. These HG and SG domains caused a two-humped gel-to-liquid phase transition in the DPPC MLVs. This report confirms the success in our first step of developing the model nanoparticle system for future *in vivo* cancer therapy.

CONFLICT OF INTEREST

Authors (GG and LP) assure no conflict of interest in this report.

REFERENCES

1. Loo C, Lowery A, Halas N, West J, Drezek R. (2005). Immunotargeted nanoshells for integrated cancer imaging and therapy. Nano Lett. 5: 709-711.

2. Huang X, Jain PK, El-Sayed IH, El-Sayed MA. (2006). Determination of the minimum temperature required for selective photothermal destruction of cancer cells with the use of immunotargeted gold nanoparticles. Photochem Photobiol. 82: 412-417.
3. Mahmoudi M, Sant S, Wang B, Laurent S, Sen T. (2011). Superparamagnetic iron oxide nanoparticles (SPIONs): development, surface modification and applications in chemotherapy. Adv Drug Delivery Rev. 63: 24-46.
4. Kah JCY, Chen J, Zubieta A, Hamad-Schifferli K. (2012). Exploiting the Protein Corona around Gold Nanorods for Loading and Triggered Release. ACS Nano. 6: 6730-6740.
5. Carnovale C, Bryant G, Shukla R, Bansal V. (2016). Size, shape and surface chemistry of nano-gold dictate its cellular interactions, uptake and toxicity. Prog Mater Sci. 83: 152-190.
6. Ghosh G, Mukherjee A, Bhilwade HN, Gupta A, Korde A, et al. (2018). Selective Cytotoxicity of Counterion-Conjugated Charged Iron Oxide Nanoparticles: A Study with Lymphoblastoid Raji Cells. J Adv Nanomater. 3: 45-56.
7. Torrano AA, Pereira ÂS, Oliveira ON Jr., Barros-Timmons A. (2013). Probing the interaction of oppositely charged gold nanoparticles with DPPG and DPPC Langmuir monolayers as cell membrane models. Colloids Surf B. 108: 120-126.
8. Michel R, Gradzielski M. (2012). Experimental Aspects of Colloidal Interactions in Mixed Systems of Liposome and Inorganic Nanoparticle and Their Applications. Int J Mol Sci. 13: 11610-11642.
9. Montis C, Generini V, Boccalini G, Bergese P, Bani D, et al. (2018). Model lipid bilayers mimic non-specific interactions of gold nanoparticles with macrophage plasma membranes. J. Colloid Interface Sci. 516: 284-294.
10. Pattani A, Patravale VB, Panicker L, Potdar PD. (2009). Immunological effects and membrane interactions of chitosan nanoparticles. Mol Pharmaceutics. 6: 345-352.
11. Akbarzadeh A, Rezaei-Sadabady R, Davaran S, Joo SW, Zarghami N, et al. (2013). Liposome: classification, preparation, and applications. Nanoscale Res Lett. 8: 102.
12. Hoffmann I, Michel R, Sharp M, Holderer O, Appavou MS, et al. (2014). Softening of phospholipid membranes by the adhesion of silica nanoparticles - as seen by neutron spin-echo (NSE). Nanoscale. 6: 6945-6952.
13. Montis C, Maiolo D, Alessandri I, Bergese P, Berti D. (2014). Interaction of nanoparticles with lipid membranes: a multiscale perspective. Nanoscale. 6: 6452-6457.
14. Pfeiffer T, De Nicola A, Montis C, Carlà F, van der Vegt NFA, et al. (2019). Nanoparticles at Biomimetic Interfaces: Combined Experimental and Simulation Study on Charged Gold Nanoparticles/Lipid Bilayer Interfaces. J Phys Chem Lett. 10: 129-137.
15. Simonelli F, Bochicchio D, Ferrando R, Rossi G. (2015). Monolayer-Protected Anionic Au Nanoparticles Walk into Lipid Membranes Step by Step. J Phys Chem Lett. 6: 3175-3179.
16. Sinha S, Jing H, Sachar HS, Das S. (2017). Role of plasma membrane surface charges in dictating the feasibility of membrane-nanoparticle interactions. Appl Phys Lett. 111: 263702.
17. Jing H, Sinha S, Sachar HS, Das S. (2019). Interactions of gold and silica nanoparticles with plasma membranes get distinguished by the van der Waals forces: Implications for drug delivery, imaging, and theranostics. Colloids Surf B. 177: 433-439.
18. Piosik E, Zaryczniak A, Mylkie K, Ziegler-Borowska M. (2021). Probing of Interactions of Magnetite Nanoparticles Coated with Native and Aminated Starch with a DPPC Model Membrane. Int J Mol Sci. 22: 5939.
19. Vorobyov I, Olson TE, Kim JH, Koeppe RE, Andersen OS, et al. (2014). Ion-induced defect permeation of lipid membranes. Biophysical Journal. 106: 586-597.
20. Biltonen RL, Lichtenberg D. (1993). The use of differential scanning calorimetry as a tool to characterize liposome preparations. Chem Phys Lipids. 64: 129-142.
21. Drazenovic J, Wang H, Roth K, Zhang J, Ahmed S, et al. (2015). Effect of lamellarity and size on calorimetric phase transitions in single component phosphatidylcholine vesicles. Biochimica et Biophysica Acta. 1848: 532-543.
22. Ghosh G, Panicker L, Ningthoujam RS, Barick KC, Tewari R. (2013). Counter ion induced irreversible denaturation of hen egg white lysozyme upon electrostatic interaction with

iron oxide nanoparticles: A predicted model. Colloids Surf B. 103: 267-274.

23. Ghosh G, Panicker L, Barick KC. (2014). Protein nanoparticle electrostatic interaction: Size dependent counterions induced conformational change of hen egg white lysozyme. Colloids Surf B. 118: 1-6.
24. Ghosh G. (2015). Counterion effects in protein nanoparticle electrostatic binding: a theoretical study. Colloids Surf B. 128: 23-27.
25. Ghosh G, Panicker L. (2021). Protein-nanoparticle interactions and a new insight. Soft Matter. 17: 3855-3875.
26. Kadu K, Ghosh G, Panicker L, Kowshik M, Roy Ramanan S. (2019). Role of surface charges on interaction of rod-shaped magnetic hydroxyapatite nanoparticles with protein. Colloids Surf B. 177: 362-369.
27. Suk JS, Xu Q, Kim N, Hanes J, Ensign LM. (2016). PEGylation as a strategy for improving nanoparticle-based drug and gene delivery. Adv. Drug Deliv Rev. 99: 28-51.
28. Shi L, Zhang J, Zhao M, Tang S, Cheng X, et al. (2021). Effects of polyethylene glycol on the surface of nanoparticles for targeted drug delivery. Nanoscale. 13: 10748-10764.
29. Sanchez-Cano C, Carril M. (2020). Recent Developments in the Design of Non-Biofouling Coatings for Nanoparticles and Surfaces. Int J Mol Sci. 21: 1007.
30. Rahme K, Dagher N. (2019). Chemistry Routes for Copolymer Synthesis Containing PEG for Targeting, Imaging, and Drug Delivery Purposes. Pharmaceutics. 11: 327.
31. Mason JT. (1998). Investigation of phase transitions in bilayer membranes. Methods in Enzymology. 295: 468-494.
32. Iswanti FC, Nurulita I, Djauzi S, Sadikin M, Witarto AB, et al. (2019). Preparation, characterization, and evaluation of chitosan-based nanoparticles as CpG ODN carriers. Biotechnology & Biotechnological Equipment. 33: 390-396.
33. Dyawanapelly S, Jagtap DD, Dandekar P, Ghosh G, Jain R. (2017). Assessing safety and protein interactions of surface-modified iron oxide nanoparticles for potential use in biomedical areas. Colloids Surf B. 154: 408-420.
34. Aswal VK, Kohlbrecher J, Goyal PS, Amenitsch H, Bernstorff S. (2006). Counterion condensation on charged micelles in an aqueous electrolyte solution as studied with combined small-angle neutron scattering and small-angle x-ray scattering. J Phys Condens Matter. 18: 11399-11410.
35. Bhandary S, Sultana P, Basu R, Das S, Nandy P. (2011). A Study on the Modulation of the Phase Behavior of Lipid Aggregates-Effect of Some Metal Nanoparticles. Adv Sci Eng Med. 3: 213-218.
36. Chibowski E, Szcześ A. (2016). Zeta potential and surface charge of DPPC and DOPC liposomes in the presence of PLC enzyme. Adsorption 22: 755-765.
37. Santhosh PB, Penič S, Genova J, Iglič A, Kralj-Iglič V, et al. (2012). A study on the interaction of nanoparticles with lipid membranes and their influence on membrane fluidity. J Phys Conf Ser. 398: 012034.
38. Deamer DW, Bramhall J. (1986). Permeability of lipid bilayers to water and ionic solutes. Chem Phys Lipids. 40: 167-188.
39. Paula S, Volkov AG, Deamer DW. (1996). Permeation of protons, potassium ions, and small polar molecules through phospholipid bilayers as a function of membrane thickness. Biophysical Journal. 70: 339-348.
40. Paula S, Volkov AG, Deamer DW. (1998). Permeation of halide anions through phospholipid bilayers occurs by the solubility-diffusion mechanism. Biophysical Journal. 74: 319-327.
41. De SK, Kanwa N, Ahamed M, Chakraborty A. (2018). Spectroscopic evidence for hydration and dehydration of lipid bilayers upon interaction with metal ions: a new physical insight. Phys Chem Chem Phys. 20: 14796-14807.
42. Yang J, Jin J, Li S. (2021). RSC Advances. Role of polyunsaturated phospholipids in liquid-ordered and liquid-disordered phases. 11: 27115-27120.
43. Bangham AD, Standish MM, Watkins JC. (1965). Diffusion of univalent ions across the lamellae of swollen phospholipids. J Mol Biol. 13: 238-252.
44. Li C, Lin D, Zhao W. (2020). Electric Field Induced Dewetting of Hydrophobic Nanocavities at Ambient Temperature. Nanomaterials. 10: 736.

45. Klesse G, Tucker SJ, Sansom MSP. (2020). Electric Field Induced Wetting of a Hydrophobic Gate in a Model Nanopore Based on the 5-HT3 Receptor Channel. ACS Nano. 14: 10480-10491.

46. Leekumjorn S, Sum AK. (2006). Molecular Simulation Study of Structural and Dynamic Properties of Mixed DPPC/DPPE Bilayers. Biophys. J. 90: 3951-3965.